In situ imaging of ultra-fast loss of nanostructure in nanoparticle aggregates

Garth C. Egan,[1] Kyle T. Sullivan,[2] Thomas LaGrange,[2] Bryan W. Reed,[2] and Michael R. Zachariah[3,4,a)]

[1]*Department of Materials Science, University of Maryland, College Park, Maryland 20742, USA*
[2]*Physical and Life Sciences Directorate, Lawrence Livermore National Laboratory, 7000 East Avenue, Livermore, California 94550, USA*
[3]*Department of Chemical and Biomolecular Engineering, University of Maryland, College Park, Maryland 20742, USA*
[4]*Department of Chemistry and Biochemistry, University of Maryland, College Park, Maryland 20742, USA*

(Received 12 December 2013; accepted 17 February 2014; published online 25 February 2014)

The word "nanoparticle" nominally elicits a vision of an isolated sphere; however, the vast bulk of nanoparticulate material exists in an aggregated state. This can have significant implications for applications such as combustion, catalysis, and optical excitation, where particles are exposed to high temperature and rapid heating conditions. In such environments, particles become susceptible to morphological changes which can reduce surface area, often to the detriment of functionality. Here, we report on thermally-induced coalescence which can occur in aluminum nanoparticle aggregates subjected to rapid heating (10^6–10^{11} K/s). Using dynamic transmission electron microscopy, we observed morphological changes in nanoparticle aggregates occurring in as little as a few nanoseconds after the onset of heating. The time-resolved probes reveal that the morphological changes initiate within 15 ns and are completed in less than 50 ns. The morphological changes were found to have a threshold temperature of about 1300 ± 50 K, as determined by millisecond-scale experiments with a calibrated heating stage. The temperature distribution of aggregates during laser heating was modeled with various simulation approaches. The results indicate that, under rapid heating conditions, coalescence occurs at an intermediate temperature between the melting points of aluminum and the aluminum oxide shell, and proceeds rapidly once this threshold temperature is reached. © *2014 AIP Publishing LLC*. [http://dx.doi.org/10.1063/1.4867116]

I. INTRODUCTION

While there are many processing methods that form isolated nanoparticles,[1,2] aggregates are prevalent in many applications as both intentional assemblies for beneficial properties[1] and unavoidable artifacts of most commercially viable synthesis techniques.[3,4] Although stabilizing agents can be used to mitigate aggregation, they typically decompose or volatilize at elevated temperatures.[5–7] While particle size is commonly reported as the average size of the primary particles, the behavior, be it mechanical, optical, or chemical, of nanoparticulate material will likely be impacted by the size and morphology of the aggregates. Furthermore, in high temperature applications aggregated nanoparticles will be thermodynamically driven to coalesce (or sinter)[8] to produce characteristically larger particles which, depending on the material properties and transport time scale of this process, could be rapid and precede the intended nanomaterial dynamics. While coalescence may be desirable in certain applications, such as bottom-up fabrication[9,10] or as a sensing method,[11] for many other applications, which demand a large surface to volume ratio, the loss of surface area caused by coalescence will decrease a material's effectiveness.[1,2] Whether one is trying to exploit or prevent coalescence and sintering, it is important to have a good understanding of the mechanisms, including the threshold temperature, the time scale, and the effect of aggregate size and morphology associated with this process.

While there has been extensive study of sintering mechanisms at moderate temperatures and over long periods,[5,6,11–13] these results are not necessarily scalable to much higher heating rates where the time scale of thermal and mechanical relaxation may become comparable, or even slower than, the characteristic heat transfer time scale. This becomes a concern in applications such as those involving optical excitation[14,15] and exothermic reactions,[16–19] where materials are subjected to rapid heating and will thermodynamically be driven to coalesce to minimize the free energy through the reduction of surface area. In such cases, the transient evolution is poorly understood due to the experimental difficulties associated with probing the very small length and time scales inherent to these processes. As a result, not much is known about the dominant mechanisms governing aggregate coalescence in this regime, or their individual time scales. Recent advances in *in situ* diagnostic techniques, such as dynamic transmission electron microscopy (DTEM),[20–23] have enabled the visualization and measurement of phase transitions and nanostructural evolution on otherwise unachievable length and time scales. Further, since DTEM utilizes laser heating, very rapid (10^{11} K/s) thermal heating rates can be applied. Thus, the technique is well suited to probe the processes associated with nanoparticle coalescence and sintering under rapid heating.

For this study, aluminum nanoparticles (Al-NPs) serve as a valuable and interesting test material, because of their wide availability and common use in a variety of material applications such as hydrolysis, sensing, nanocomposites,

a)Author to whom correspondence should be addressed. Electronic mail: mrz@umd.edu

and solar cells.[24–28] One promising application for aluminum is as a high energy density fuel in combustion, propellants, or explosive formulations.[16,29–31] In these applications, aluminum particles undergo rapid heating, and it is critical to understand the onset temperature and time scale of coalescence, as these parameters will directly impact the mechanism of oxidation. For example, if the coalescence time scale is significantly faster than the combustion time scale, then aggregates will coalesce prior to combustion. This would warrant the need for a different combustion model than if the aggregate burned as an ensemble of individual nanoparticles. When exposed to air, aluminum particles form a 2–5 nm amorphous oxide shell.[16,17,29–32] While such thin oxide layers are common to most metal particles, and often insignificant on large scales, they can dominate the behavior when the particles are small and the shell is a substantial fraction of the volume. Aluminum has a melting temperature of 933 K, while the aluminum oxide melts at 2327 K. Upon melting, the aluminum will undergo a volumetric expansion (~6 vol. %), while the oxide shell will remain solid. The resultant mechanical and thermal stresses will govern the material's behavior—a point that has led to conflicting opinions about the material dynamics occurring upon rapid heating.[17,32] In particular, it has been theorized that these stresses can induce material rupture in a process termed melt dispersion, leading to the unloading of high-velocity molten aluminum droplets which can then be oxidized.[17] The thermal ramp ($>10^6$ K/s) provided by DTEM can allow for the direct experimental examination of these theories.

Herein, we report on the *in-situ* heating of aluminum nanoparticle aggregates at rates of 10^6–10^{11} K/s, and the morphological changes that result. The use of DTEM allows for both qualitative visualization of the nanostructural evolution of aggregates and direct measurement of the time scale associated with this process. Modeling and more conventional *in situ* TEM measurements are also included and provide a more straightforward measurement of the temperature dependence. The results are used to draw conclusions about the onset temperature, time scale, and possible mechanisms driving the coalescence event in core-shell nanoparticle aggregates. In particular, we show that the sudden rupturing and dispersal necessary for the melt dispersion mechanism does not occur even up to heating rates much higher than those typical of combustion.

II. EXPERIMENTAL DETAILS

Samples were prepared by adding 5 mg of Al-NPs (80 nm primary particle size, Novacentrix) to a vial with 10 ml of EtOH. Previous thermogravimetric analysis measured the active content of the Al to be 73 wt. %, with the other 27 wt. % representing the oxide shell. The slurry was ultrasonicated for several minutes and then pipetted onto a TEM grid. Two types of grids were used, including Formvar-coated copper grids as well as silicon nitride membrane grids (SPI supplies).

Experiments were performed using the DTEM at Lawrence Livermore National Laboratory (LLNL), the details of which have been previously reported.[20–23] The DTEM is a TEM equipped with a pulsed laser which strikes the cathode and leads to the photoemission of ~10^9 electrons, allowing an image to be captured with a ~15 ns exposure time (roughly equal to the pulse width of the cathode laser). A second sample drive laser (1064 nm wavelength) is used to induce rapid heating of the sample, and this is synchronized with the electron pulse plus or minus an adjustable delay. Zero delay corresponds to the time when the peak intensities of both pulses are coincident at the sample. Due to the limited electron source brightness and stochastic electron-electron scattering during transit down the TEM column, the images taken with these 15 ns electron pulses are inevitably less resolved than an image taken with a continuous wave (CW) thermionic source used in conventional TEM. While this is a necessary sacrifice for temporal resolution, the spatial resolution of the pulse images is sufficient to observe the morphological transition of interest to this study. However, as the DTEM is capable of operating in both modes (pulsed and CW), images were also taken in CW mode to provide detail on the finer structural changes of the samples.

Further experiments were preformed with the Protochips Inc. Aduro stage with silicon nitride coated e-chips, which allowed for *in situ* heating at rates up to ~10^6 K/s. Modeling of the aggregate temperatures was also performed using both T-matrix[33,34] and finite element approaches. The details of this can be found in the Supplemental Material.[35]

III. RESULTS AND DISCUSION

The general effect of high heating rates on the morphology of Al-NP aggregates can be seen with the CW images in Figure 1, which show an aggregate heated *in-situ* with 12 ns laser pulses (~10^{11} K/s). Fig. 1(a) shows the aggregate of approximately 100 nanoparticles with average size of 80 nm prior to heating, and Fig. 1(b) shows that aggregate after a single heating pulse. Each subsequent image (Figs. 1(c)–1(h)) shows the morphological evolution of the aggregate after additional laser pulses. As can be seen from these images, the heating led to significant morphological changes in the aggregate which can be described as the coalescence of the discrete nanoparticles into larger structures. This change in size corresponds to a loss of surface area, which is estimated to be ~40% from Figs. 1(a) and 1(b) (see Supplemental Material on the details of this estimation[35]). This process continues through the rest of the series of pulses but with markedly diminished amounts of change after each additional pulse. Compared to that initial loss of 40%, the subsequent total loss only reaches 65% up through Fig. 1(f), after which continued heating resulted in the loss of mass by evaporation. As a point of reference, complete sintering of the aggregate into a single sphere would correspond to roughly a 78% loss in surface area (i.e., with $n_1 \sim 100$ and $n_2 = 1$, as defined in the Supplemental Material).

Time-resolved experiments were conducted by acquiring three images of the aluminum nanoparticle aggregates; before laser heating, during heating, and after cooling to visualize the final morphology. Complementary conventional CW TEM images of the clusters were obtained before and after laser heating to assist the interpretation of the pulsed

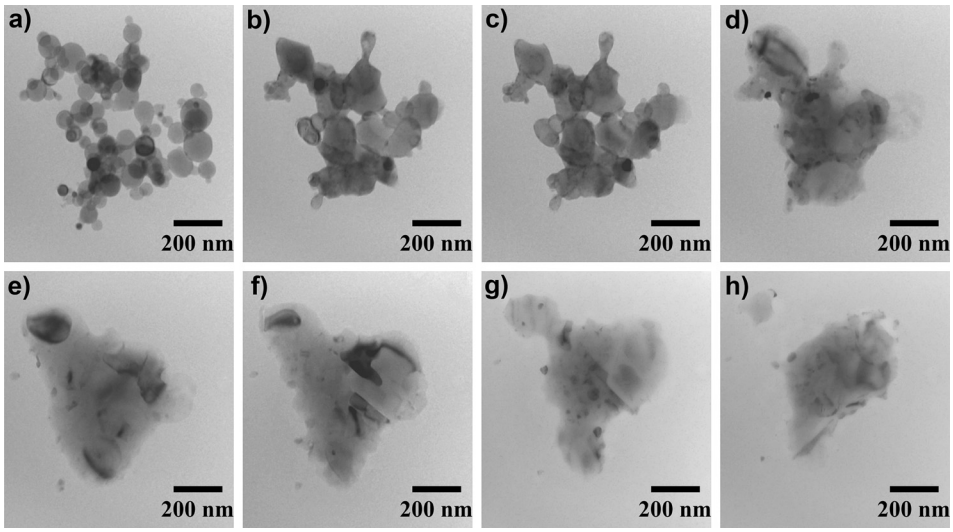

FIG. 1. An aggregate of Al-NPs before (a) and after (b–h) successive heating with 12 ns laser pulses with fluence 1.23 kJ/m^2. Images were taken with the DTEM in CW mode with long pauses between pulses for the taking of the micrographs.

mode images. We performed such experiments on multiple sample regions, containing a total of ~50–100 such clusters for each of the various experimental parameters to establish a reasonable sample size. Figure 2 is a series of time-resolved images and micrographs taken in CW mode (Figs. 2(a) and 2(b)), showing the change in the nanostructure character of the aggregate before and after heating with a single laser pulse. The laser fluences for these experiments (1.52 kJ/m^2) were slightly higher than those used to produce Fig. 1 (1.23 kJ/m^2), leading to a higher degree of coalescence. After one pulse, most of the aggregate's nanostructure character has been lost, reducing the surface area by approximately 68% (details are described in Supplemental Material[35]). Though having low signal to noise ratios, the time resolved images of Figs. 2(c)–2(e) show the general trend in coalescence behavior with rapid pulsed laser heating and can be compared with conventional TEM images in Figs. 2(a) and 2(b). Within the 12 ns period of the laser pulse (i.e., 0 time delay in which the temporal peaks of the electron and laser heating pulses coincide at the sample position), the cluster undergoes significant coalescence and loses its nanoscale features. The experiment shown in Fig. 2 was repeated with various delays, ranging from −20 ns to 150 ns. As expected, at times before −10 ns, no coalescence was observed, confirming the calibration of time zero. For delays 50 ns and greater, no significant morphological differences were observed between the intermediate and after images, indicating that coalescence completes in less than 50 ns for a single shot.

Complementary to the laser heating experiments, we also conducted *in-situ* TEM studies of nanoparticle coalescence using a high heating rate TEM stage based on small-mass micromachined heaters (Aduro, Protochips Inc.), which resistively heats a silicon nitride (SiN_x) substrate at rates as high as 10^6 K/s.[36] Samples were heated to various temperatures at 10^6 K/s, held at temperature for 1 ms, and then quenched, cooling at approximately the same rate. Interestingly, the threshold temperature for coalescence was not the melting point of either the aluminum core (933 K) or the oxide shell (2327 K) but an intermediate temperature of 1300 ± 50 K in agreement with previous work.[18] Figures 3(a) and 3(b) show the before and after images of a sample heated to 1173 K. Several particles show a large change in contrast after being heated, consistent with melting and resolidification of the

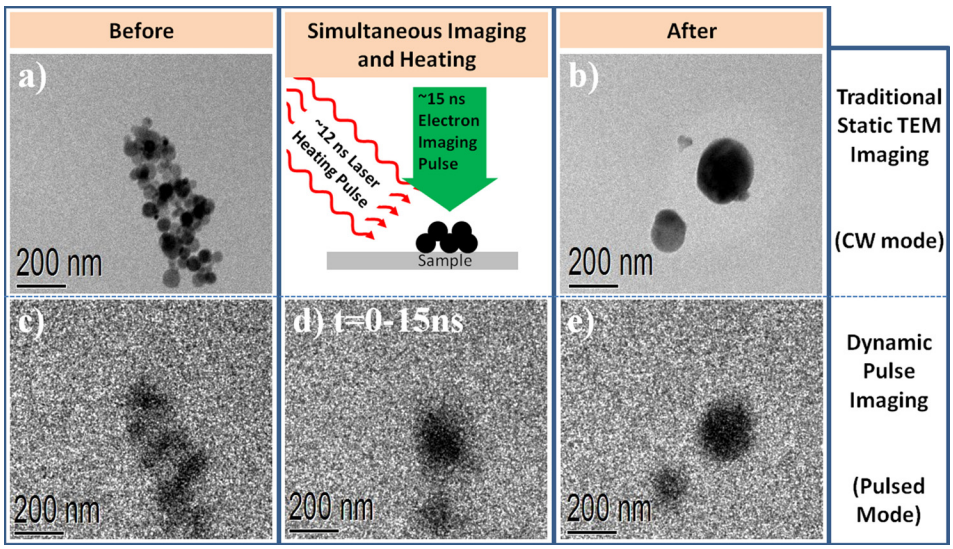

FIG. 2. An aggregate of Al-NPs before (a,c), during (d), and after (b,e) a 12 ns sample drive laser pulse of 1.52 kJ/m^2. Images a and b were taken with the DTEM in CW mode and images (c–e) were taken with time resolved pulse mode. The intermediate image (d) was taken with a 0 ns delay from the initiation of the heating pulse

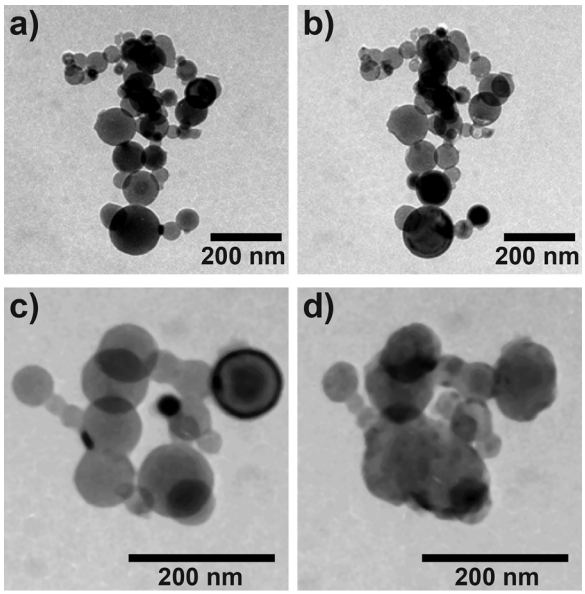

FIG. 3. An aggregate of Al-NPs before (a,c) and after (b,d) heating with the hot stage to high temperatures and being held there for 1 ms. The aggregates in (a,b) and (c,d) were heated to 1173 K and 1323 K, respectively. The images were taken with the DTEM in CW mode. Note that for images a and b, while no coalescence has occurred, there are significant changes in contrast (most obvious in the group of 5 nanoparticles towards the bottom of the images), which suggests that there was melting in the metal cores. This is in contrast to images (c,d) where significant morphological change is obvious.

aluminum core, though there was no indication of significant coalescence. Only upon heating to temperatures of 1323 K (Figs. 3(c) and 3(d)) were notable morphological changes observed, with multiple particles coming together to form larger particles in a manner qualitatively similar to Fig. 1.

While having a threshold temperature at relatively low heating rates provides a lower bound estimate for the coalescence temperatures involved with the laser heating experiments, a deeper understanding of aggregate temperature is desired. To this end, we employed several approaches to model the laser absorption process. While the optical properties of aluminum are well known,[37] the near-field interaction of the light with the fractal aggregate shapes and support films can be complex and non-uniform[33] making accurate temperature data difficult to calculate. This type of interaction leads to local enhancement in absorption[33] and can cause hotspots in the aggregate which could act as initiation points for sintering. The necessity of these hotspots is revealed by first considering the aggregate as a group of non-interacting isolated spheres and calculating their absorption through Mie theory. This approach gives peak temperatures of only 550 K, well below both the melting point of Al and the observed 1300 K threshold for sintering.[18] To understand the absorption of the aggregate on the whole, we employed Mackowski's Multiple Scattering T-matrix Code[33,34] for generalized fractal aggregates. Modeling details and theory can be found in the Supplemental Material.[35] This modeling showed the range of absorption efficiencies that exist in an aggregate, with those particles in the most densely packed areas absorbing far more than the rest.

To correlate absorption hotspots with spatial variation in temperature, one must account for heat transfer between particles and to the supporting film within the period that the nanosecond pulse hits the sample, as well as for other factors not considered in the T-matrix calculation, such as the oxide shell. For this, we employed finite-element simulations in COMSOL™. While corroborating the need for multiple particles and hotspots to reach the sintering threshold, these simulations showed that peak temperature was highly dependent on both the exact sizes and shapes of the gaps between spheres (see Figure S3(b)) and the laser absorption properties of the substrate. Further, we found that the oxide layer does have an effect, albeit a relatively small one. More detail on these results can be found in the Supplemental Material.[35]

The models are in good agreement with the experimental results and help explain why, under the same heating pulse, larger aggregates were far more likely to coalesce than small (<10 particles) aggregates, such as in Figure 4. This is likely because larger aggregates have more particle-particle interfaces and are much more likely to feature hotspots and will, relative to their masses, lose heat to the substrate much more slowly. However, the model results also indicate that the laser absorption and peak temperature change can only be predicted to a fairly rough approximation, with values varying by a factor of ~2–3 or more depending on the details of the size and shape of the Al-NP aggregate, the precise geometry of the hot spots, and the contact points between the aggregate and the substrate. While these quantities can be determined experimentally to some extent, for example by tomographic reconstruction, the nanometer precision required for characterization of the hot spot geometries is exceedingly challenging. Indeed this wide variation in temperature response is supported by the experimental observation which shows superficially similar aggregates

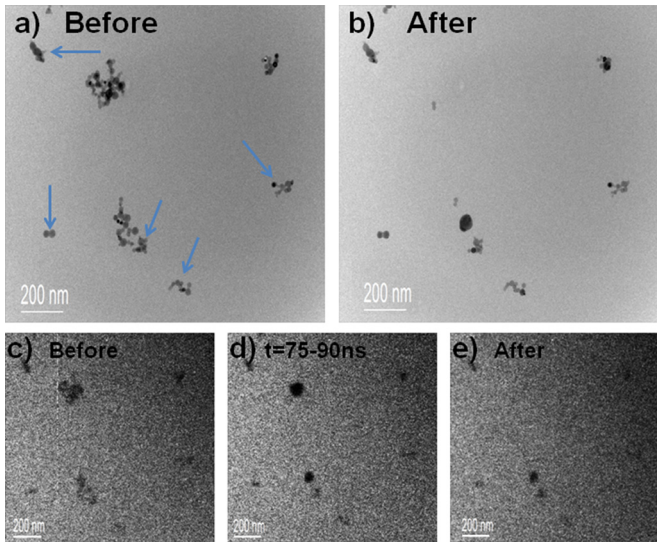

FIG. 4. Aggregates of Al-NPs before (a,c), during (d), and after (b,e) a 12 ns sample drive laser pulse of 1.52 kJ/m^2. Images (a,b) were taken with the DTEM in CW mode and (c,d) were taken with time resolved pulse mode. The intermediate image, B, was taken with a 75 ns delay from the initiation of the heating pulse. These images illustrate the disparate response of aggregates to the same heating pulse, and how large aggregates are far more likely to coalesce than the smaller ones. The arrows show ones that did not change from the heating laser pulse.

behaving differently when exposed to identical laser pulses (see Fig. 4). However, we can still estimate upper bound temperatures using the T-matrix calculation for a specific aggregate with the assumptions that there are no spaces between the metallic spheres (i.e., they meet at tangent points, which maximizes the intensity of a hot spot assuming all particles are spherical) and that heat loss to the substrate is negligible on the 12 ns time scale of heating. By this metric, the upper bounds for the temperatures achieved for the aggregates in Figs. 1 and 2 are 1310 K and 1690 K, respectively. The details behind these calculations can be found in the Supplemental Material.[35]

These results allow us to draw some conclusions about the sintering behavior of Al-NPs. Foremost is that coalescence begins within ~10 ns of the onset of rapid heating and is essentially complete within ~50 ns. The threshold temperature for sintering at high heating rates is 1300 K, which is between the melting points of the metal core and the metal oxide shell. This result provides direct experimental evidence that the volumetric expansion upon melting is not sufficient to cause spallation of the aluminum oxide shell, which is the main premise behind the melt dispersion mechanism.[17] Also, the lack of any evidence for spallation and the qualitatively similar results for both laser and resistive stage heating, despite the several orders of magnitude difference in the heating rates, further conflicts with the occurrence of such a mechanism. Alternatively, sintering may result from aluminum diffusing through or into the oxide shell along with oxygen diffusing into the core.[38,39] This could produce a reduced oxide, thereby softening the oxide shell and lowering its melting point and removing it as a barrier to coalescence. Such a process has been predicted to occur on the nanosecond time scale in molecular dynamic simulations[40] but would require very fast diffusion rates (effective diffusivity of $\sim 10^{-9}$ m^2/s for Al and O to pass through 2–3 nm oxide shell faster than the ~10 ns time scale of sintering). Such high diffusivity may be achieved at higher temperatures, and if the process is assisted by the electric field developed from the charge imbalance between the oxide shell and core, i.e., a Cabrera-Mott mechanism.[38] In the case of laser heating, the physics is further complicated by the large oscillatory electric fields present in the hot spots, which can reach 10^8–10^9 V/m (see Supplemental Material[35]).

Another possibility is that the rapid coalescence observed under high heating rates may result from the formation of microfractures[41] in the shell, through which the molten Al core can flow and promote coalescence with the surrounding material. As our results show that the shell is not left behind as an empty container, such fracturing would not just let the core escape but would also have to promote the motion of the shell. This could occur through faster reduction of the shell once in contact with Al from both sides to create a lower melting, reduced oxide or if fractured into small enough pieces the shell could be pulled along with the flow of the molten core. The later possibility may account for the irregular and rough shapes found in Fig. 3(d) and the later images of Fig. 1. A fracturing mechanism would operate under conditions of rapid heating in which both the hoop stresses in oxide are large and the oxide layer is softened due to the elevated temperatures. On length scales of only a few nanometers of aluminum oxide shell, failure of the oxide should be much faster compared to all other time scales. The threshold temperature would thus represent the point of sufficient stress and softening to allow this process to occur. Such a mechanism could explain why, in comparing the results of Fig. 1 (laser heating, 10^{11} K/s) and Figs. 3(c) and 3(d) (resistive stage heating, 10^6 K/s), the morphological changes are qualitatively similar despite the five orders of magnitude difference in heating rates and 2–3 orders of magnitude difference in cooling times (ms vs. multiple μs). If the coalescence were governed by a gradual process, one would expect more morphological changes in a material held at temperature for much longer. As this is not the case, a rapid mechanism, such as the one described, occurring at a defined threshold temperature seems more likely.

In combustion applications, fast coalescence has the potential to inhibit or enhance reactivity depending on the nature of the reaction. If the aluminum is isolated from other materials such that the oxidizer delivery rate is slow relative to the coalescence, then particle growth will precede the bulk of the reaction. This is particularly relevant for aluminum particles oxidizing in a gaseous environment. Bazyn *et al.*[42] have measured burn times of aluminum on the order of tens of microseconds, even in a pressurized oxygen environment. Our results suggest that the particles may coalesce well before they significantly combust. This could explain the diminishing returns to burn times from reducing the size of Al particles,[30,43] as they can coalesce into larger particles prior to combustion, and thus do not retain the high surface-to-volume ratios needed for increased combustion rates. However, if the fuel is not isolated and is instead intimately mixed with nanoparticle oxidizer, fast sintering can facilitate the reaction by rapidly exposing a high surface area of molten fuel to the surrounding nanoparticle oxidizer matrix. Rather than coalescing towards a sphere, the mobile fuel could wet the contacted oxidizer, thereby increasing the amount of interfacial area and thus the reactivity, on time scales of ~10 ns. In the case of nanocomposite thermites (i.e., Al + CuO) in which nanoparticles of a metal oxide are mixed with the aluminum fuel, such a mechanism would support previous reports that the reaction proceeds, in part, via a reactive sintering mechanism.[18]

IV. CONCLUSION

In-situ, high heating rate experiments on aluminum nanoparticle aggregates revealed that the nanostructure of the samples severely coarsened upon heating in a manner consistent with simple coalescence driven by the reduction of surface energy. When subjected to heating rates of 10^{11} K/s, aggregates were substantially coarsening within ~15 ns from the start of heating, and all significant changes were complete within 50 ns. Using a heating stage, we found the threshold temperature for coarsening to be around 1300 K, with qualitatively similar morphological changes despite a five order of magnitude difference in heating rate,

indicating similar mechanisms taking place on the nanosecond and sub-millisecond scales.

These results allowed us to qualitatively assess the relevance of different mechanisms proposed for rapid combustion of Al-NP aggregates. Specifically, a mechanism resulting from the pressure induced spallation of the molten core of aluminum nanoparticle seems very unlikely, given that no such behavior was observed even at heating rates much faster than those typical for rapid combustion. Rather, the early-stage evolution appears to be a simple surface-energy-driven coarsening process, facilitated perhaps by fracturing or softening (via thermal and/or interdiffusion mechanisms) of the oxide shells. This coarsening process is sufficiently fast (~50 ns to completion given sufficient heating rates) to alter the combustion kinetics and reduce reaction rates by decreasing the surface area to volume ratio of the nanoparticle aggregates. This may help to explain the deviations from expected scaling of combustion rate with particle size and lower than expected reaction rates at particle diameters below ~100 nm. The observed phenomena and insight gained by these studies may extend to other applications. For example, given the short pulses that are sometimes used for optical excitation of nanoparticles, such as in hyperthermia and spectroscopy, the peak temperatures may be considerably higher than expected due to absorption hot spots in dense aggregates and the inability to conduct sufficient heat into the surroundings during the short time scale. This could lead to unexpected sintering and thus the loss of nanoscale structure. In short, competition between fast coalescence, which reduces the advantageous properties of nanoparticle systems, and reactions must be considered in the design and implementation of nanomaterials.

ACKNOWLEDGMENTS

Experimental work was performed at Lawrence Livermore National Laboratory under the auspices of the United States Department of Energy by Lawrence Livermore National Laboratory under Contract W-7405-Eng-48 and was supported in part by the US DOE Office of Basic Energy Sciences, Division of Materials Sciences and Engineering under FWP-SCW0974. Work by BWR was supported by the US DOE Office of Basic Energy Sciences, Division of Materials Sciences and Engineering under FWP-SCW0974. Work by T.L. was supported by DTRA grant. Support for G.C.E. and M.R.Z. was from the Army Research Office.

[1]Y. J. Min, M. Akbulut, K. Kristiansen, Y. Golan, and J. Israelachvili, Nat. Mater. **7**, 527 (2008).
[2]B. L. Cushing, V. L. Kolesnichenko, and C. J. O'Connor, Chem. Rev. **104**, 3893 (2004).
[3]P. C. Hiemenz and R. Rajagopalan, *Principles of Colloid and Surface Chemistry, Revised and Expanded* (CRC Press, 1997).
[4]F. E. Kruis, H. Fissan, and A. Peled, J. Aerosol Sci. **29**, 511 (1998).
[5]Y. Chen, R. E. Palmer, and J. P. Wilcoxon, Langmuir **22**, 2851 (2006).
[6]L. Meli and P. F. Green, Acs Nano **2**, 1305 (2008).
[7]R. Prasher, P. E. Phelan, and P. Bhattacharya, Nano Lett. **6**, 1529 (2006).
[8]The process discussed in this paper involves core-shell particles and the transport involving both liquid Al and solid Al_2O_3. As a result, the strictest definitions of both sintering and coalescence are not fully descriptive of the coarsening mechanism. However, we feel coalescence is a broader term and thus it is primarily used to refer to this process.
[9]J. W. Chung, S. W. Ko, N. R. Bieri, C. P. Grigoropoulos, and D. Poulikakos, Appl. Phys. Lett. **84**, 801 (2004).
[10]A. Sandmann, C. Notthoff, and M. Winterer, J. Appl. Phys. **113**, 044310 (2013).
[11]T. Kim, C. H. Lee, S. W. Joo, and K. Lee, J. Colloid Interface Sci. **318**, 238 (2008).
[12]C. T. Campbell, S. C. Parker, and D. E. Starr, Science **298**, 811 (2002).
[13]A. K. Datye, Q. Xu, K. C. Kharas, and J. M. McCarty, Catal. Today **111**, 59 (2006).
[14]A. O. Govorov and H. H. Richardson, Nano Today **2**, 30 (2007).
[15]V. K. Pustovalov, Chem. Phys. **308**, 103 (2005).
[16]E. L. Dreizin, Prog. Energy Combust. Sci. **35**, 141 (2009).
[17]V. I. Levitas, Combust. Flame **156**, 543 (2009).
[18]K. T. Sullivan, N. W. Piekiel, C. Wu, S. Chowdhury, S. T. Kelly, T. C. Hufnagel, K. Fezzaa, and M. R. Zachariah, Combust. Flame **159**, 2 (2012).
[19]C. Langhammer, E. M. Larsson, B. Kasemo, and I. Zoric, Nano Lett. **10**, 3529 (2010).
[20]T. LaGrange, G. H. Campbell, B. Reed, M. Taheri, J. B. Pesavento, J. S. Kim, and N. D. Browning, Ultramicroscopy **108**, 1441 (2008).
[21]T. LaGrange *et al.*, Micron **43**, 1108 (2012).
[22]B. W. Reed, M. R. Armstrong, N. D. Browning, G. H. Campbell, J. E. Evans, T. LaGrange, and D. J. Masiel, Microsc. Microanal. **15**, 272 (2009).
[23]M. K. Santala, B. W. Reed, T. Topuria, S. Raoux, S. Meister, Y. Cui, T. LaGrange, G. H. Campbell, and N. D. Browning, J. Appl. Phys. **111**, 024309 (2012).
[24]B. Alinejad and K. Mahmoodi, Int. J. Hydrogen Energy **34**, 7934 (2009).
[25]X. Y. Huang, P. K. Jiang, and C. U. Kim, J. Appl. Phys. **102**, 124103 (2007).
[26]Y. N. Zhang, Z. Ouyang, N. Stokes, B. H. Jia, Z. R. Shi, and M. Gu, Appl. Phys. Lett. **100**, 151101 (2012).
[27]Y. Ekinci, H. H. Solak, and J. F. Loffler, J. Appl. Phys. **104**, 083107 (2008).
[28]T. L. Temple and D. M. Bagnall, J. Appl. Phys. **109**, 084343 (2011).
[29]R. A. Yetter, G. A. Risha, and S. F. Son, Proc. Combust. Inst. **32**, 1819 (2009).
[30]Y. Huang, G. A. Risha, V. Yang, and R. A. Yetter, Proc. Combust. Inst. **31**, 2001 (2007).
[31]W. K. Lewis, C. G. Rumchik, M. J. Smith, K. A. S. Fernando, C. A. Crouse, J. E. Spowart, E. A. Guliants, and C. E. Bunker, J. Appl. Phys. **113**, 044907 (2013).
[32]S. Chowdhury, K. Sullivan, N. Piekiel, L. Zhou, and M. R. Zachariah, J. Phys. Chem. C **114**, 9191 (2010).
[33]D. W. Mackowski and M. I. Mishchenko, J. Quant. Spectrosc. Radiat. Transfer **112**, 2182 (2011).
[34]D. W. Mackowski and M. I. Mishchenko (2011), http://www.eng.auburn.edu/users/dmckwski/scatcodes/.
[35]See supplementary material at http://dx.doi.org/10.1063/1.4867116 for details of the calculations and modeling referenced in this work are provided. This includes the estimation of surface area loss and the modeling of temperature under laser heating with both the T-matrix and finite-element approaches.
[36]The heating and temperature measurements are calibrated by the manufacturer. For a disperse sample using small particle sizes, it is assumed that temperature equilibrates quickly between the substrate and sample such that the temperature profile in the particles is equal to that of the SiN_x film. This assumption is based in part on the calculations in Ref. 32.
[37]D. Y. Smith, E. Shiles, and M. Inokuti, in *Handbook of Optical Constants of Solids*, edited by E. D. Palick (Academic Press, Orlando, 1985), p. 369.
[38]B. J. Henz, T. Hawa, and M. R. Zachariah, J. Appl. Phys. **107**, 024901 (2010).
[39]Y. Li, R. K. Kalia, A. Nakano, and P. Vashishta, J. Appl. Phys. **114**, 134312 (2013).
[40]P. Chakraborty and M. R. Zachariah, "Do nanoenergetic particles remain nano-sized during combustion?" Combust. Flame (in press), http://dx.doi.org/10.1016/j.combustflame.2013.10.017.
[41]D. A. Firmansyah, K. Sullivan, K. S. Lee, Y. H. Kim, R. Zahaf, M. R. Zachariah, and D. Lee, J. Phys. Chem. C **116**, 404 (2012).
[42]T. Bazyn, H. Krier, and N. Glumac, Combust. Flame **145**, 703 (2006).
[43]P. Lynch, H. Krier, and N. Glumac, Proc. Combust. Inst. **32**, 1887 (2009).